Multiresolution Time-Domain Using CDF Biorthogonal Wavelets

Traian Dogaru, *Member, IEEE,* and Lawrence Carin, *Fellow, IEEE*

Abstract—A new approach to the multiresolution time-domain (MRTD) algorithm is presented in this paper by introducing a field expansion in terms of biorthogonal scaling and wavelet functions. Particular focus is placed on the Cohen–Daubechies–Feauveau (CDF) biorthogonal-wavelet class, although the methodology is appropriate for general biorthogonal wavelets. The computational efficiency and numerical dispersion of the MRTD algorithm are addressed, considering several CDF biothogonal wavelets, as well as other wavelet families. The advantages of the biorthogonal MRTD method are presented, with emphasis on numerical issues.

Index Terms—Biorthogonal wavelets, multiresolution analysis, time-domain methods.

I. Introduction

THE multiresolution time-domain (MRTD) method has been applied successfully to various electromagnetic-field problems, such as microwave cavities and circuits [1], [2], as well as scattering by general targets [4]–[6]. It has been shown that MRTD often yields important computational savings, *vis-à-vis* the traditional finite-difference time-domain (FDTD) method [7]–[9] without sacrificing solution accuracy.

Higher order finite-difference schemes have been devised within the FDTD framework [10], [11]. However, significant issues are associated with their implementation for general scattering problems, requiring hybrid approaches for treatment of interfaces between different media, as well as for absorbing boundary conditions [11]. The MRTD achieves a multigrid structure by introducing denser discretization (scaling functions and wavelets) in zones with relatively fast spatial field variation, while keeping a lower resolution representation (scaling functions alone) in slowly varying regions. Multigrid schemes have been studied in the context of FDTD [12]–[14], but in that paper, there were difficulties in formulating a general stability criterion. By contrast, the multiresolution wavelet expansion employed by MRTD provides a natural multigrid formulation, for which rigorous stability criteria can be established. Another feature of the MRTD algorithm is that it incorporates a sub-cell methodology for treating the boundary between two dielectric media, without having to introduce a staircase approximation. In this context, an analogous formulation could be devised for the FDTD algorithm, in which the dielectric/magnetic properties of the media are averaged inside the Yee cells [9]. Summarizing, for each of the principal issues addressed by MRTD (higher order approximation of the fields, multigrid

structure, and accurate treatment of the interface between different media), there exists a more or less *ad hoc* solution within the traditional FDTD framework. However, the MRTD simultaneously addresses all of these issues, within a rigorous and stable construct.

In the MRTD algorithm, the fields are expanded in a wavelet basis [15], and Maxwell's curl equations are discretized using a method-of-moments procedure [16]. In the existing literature on MRTD, the basis functions of choice have been orthonormal wavelets from the Battle–Lemarie wavelet family [1]–[3], the Haar wavelet family [4]–[6], as well as, more recently, the Daubechies scaling functions [17], [18]. The Battle–Lemarie wavelets display good smoothness properties, but they have the disadvantage of infinite (though exponentially decaying) support. This means that many neighboring terms must be included in the update equation at each node, and that there may be numerical issues associated with the truncation of the MRTD coefficient sequence (as explained in Section III). The Haar wavelet family yields a simple algorithm. In fact, it can be shown that an n-level Haar wavelet expansion is equivalent to the Yee FDTD scheme applied to a grid of 2^n higher resolution. Unfortunately, the Haar wavelets lack smoothness. In this paper, we seek a balance between smoothness and reduced spatial support. The former addresses numerical dispersion, and the latter yields algorithmic simplicity while avoiding truncation errors.

The remainder of this paper is organized as follows. The choice of the biorthogonal wavelet family is discussed in Section II. We present the formulation of the biorthogonal MRTD scheme in Section III, using scaling functions alone, with consideration of the stability criterion and dispersion curves. Section IV performs a similar analysis of the biorthogonal MRTD scheme, including a first level of wavelet functions. In Section V, we present a simple numerical example using various versions of the MRTD algorithm. Conclusions are drawn in Section VI.

II. Choosing the Wavelet Family for Field Expansion

The main objective of the MRTD method is a minimization of the computational resources required for a given accuracy of the electromagnetic solution. In this context, we would like to reduce the number of unknowns, by decreasing the number of discretization points per wavelength, while simultaneously keeping the numerical dispersion under control. A second and distinct issue involves reduction of the total number of computations required by the algorithm (i.e., while it is generally desirable to reduce the discretization rate per wavelength, this salu-

	CDF (2,2)	CDF (2,4)	CDF (2,6)	CDF (3,3)	Cubic spline Battle-Lemarie
Scaling only	0.7500	0.6844	0.6585	0.6844	0.6371
Scaling + One Level Wavelet	0.6046	0.4831	0.4221	0.4815	0.2625

tary goal is mitigated if the associated algorithmic complexity is simultaneously increased).

The first problem can be reformulated as follows: find a wavelet basis that minimizes the numerical dispersion error of the MRTD algorithm for a given discretization rate. This is clearly related to how "good" an approximation of the fields can be obtained by considering a wavelet expansion limited to a certain number of levels. This is a typical problem encountered in data-compression techniques [15]. Let us consider the following general expansion of the function f:

$$f = \sum_{l,m} \langle f, \psi_{l,m} \rangle \, \tilde{\psi}_{l,m}. \tag{1}$$

Here, $\psi_{l,m}$ represents the wavelet function at level l, shifted by $m/2^l$ units, whereas $\tilde{\psi}_{l,m}$ is the dual of this function. They must satisfy the following orthogonality relationship:

$$\left\langle \psi_{l,m}, \tilde{\psi}_{l,m} \right\rangle = \delta\left(l - l'\right) \delta\left(m - m'\right). \tag{2}$$

If $\psi_{l,m} = \tilde{\psi}_{l,m}$, then the wavelets are orthonormal. If the basis functions are different, then the family of wavelets is biorthogonal. Two common requirements used in designing wavelet systems are regularity and vanishing moments [15]. Regularity refers to the degree of differentiability of a function, whereas the nth moment of the wavelet function is defined as $m_1(n) = \int x^n \psi(x) \, dx$. Suppose the function f is smooth and we want to approximate it by truncating the expansion in (1) to a finite number of levels. It can then be shown [15] that, in order to obtain a good approximation, we require that $\psi_{l,m}$ have as many vanishing moments as possible, and $\tilde{\psi}_{l,m}$ be as regular as possible.

An additional requirement for the wavelet system is that the expansion functions should have minimal support. As will become more evident in Sections III and IV, this condition addresses the algorithmic computational complexity. If we restrict ourselves to orthonormal wavelet systems, it can be shown that regularity and minimal support are two conflicting requirements [15]. The Battle–Lemarie family of wavelets, which are derived from B-spline functions [1], [15], have good regularity properties (depending on the order of the spline functions used in design), but they have infinite support. This results, theoretically, in an infinite number of MRTD terms in each update equation. Since the Battle–Lemarie functions display exponential decay, the higher order MRTD coefficients also decay fast. Nevertheless, truncating the sequence of MRTD coefficients [1] to a reasonable number (usually 8–12 on each side) poses problems in terms of arithmetic precision by vitiating the properties of the wavelet functions imposed by design. Reference [19] draws attention to implementation of wavelet systems in finite precision arithmetic, which can result in nonzero moments and eventually nonorthogonal systems.

Compactly supported orthonormal wavelets have been obtained by Daubechies [15] by maximizing the number of vanishing moments. The Cohen–Daubechies–Feauveau (CDF) family of biorthogonal wavelets [15] uses spline functions as dual wavelets $\tilde{\psi}_{l,m}$ and maximizes the vanishing moments of $\psi_{l,m}$ for a given extent of their support. The main difference, compared to Battle–Lemarie wavelets, is that the biorthogonal wavelets yield compact support. This means that the sequence of MRTD coefficients required in the update equations is rigorously finite (no truncation is needed).

In conclusion, the biorthogonal wavelet systems strike a good balance between regularity and reduced support. While the Battle–Lemarie wavelets are symmetric and smooth, they must be truncated to achieve finite support.

III. BIORTHOGONAL MRTD USING SCALING FUNCTIONS

A. MRTD Formulation

The derivation of the MRTD equations for a biorthogonal-wavelet field expansion is similar to the derivation for the orthogonal case [1], [6]. To keep the presentation simple, we consider one-dimensional (1-D) wave propagation with components E_z and H_y propagating in the x-direction. The full wavelet expansion of the component E_z can be written as

$$E_z(x, t) = \sum_{k,m=-\infty}^{\infty} \left[E_{k,m}^{\Phi} \tilde{\Phi}_m(x) + \sum_{l=0}^{\infty} E_{k,m}^{\Psi^l} \tilde{\Psi}_m^l(x) \right] h_k(t). \tag{3}$$

Here, we denote by $\tilde{\Phi}_m$ the dual scaling function shifted by m units, and by $\tilde{\Psi}_m^l$ the lth level dual-wavelet function displaced by $m/2^l$ units. For time discretization, we use rectangular pulses $h_k(t)$, where k represents the shift in time units. A similar equation holds for H_y, only the supports of the scaling/wavelet functions are displaced half a unit relative to E_z. In this section, we consider expansion in terms of scaling functions alone as follows:

$$E_z(x, t) = \sum_{k,m=-\infty}^{\infty} E_{k,m}^{\Phi} \tilde{\Phi}_m(x) h_k(t). \tag{4}$$

Fig. 1. Scaling and wavelet functions and their duals for several families of CDF biorthogonal wavelet systems. In all cases, the graphs are approximations obtained by the cascade algorithm after eight iterations. (a) CDF $(2, 2)$. (b) CDF $(2, 4)$.
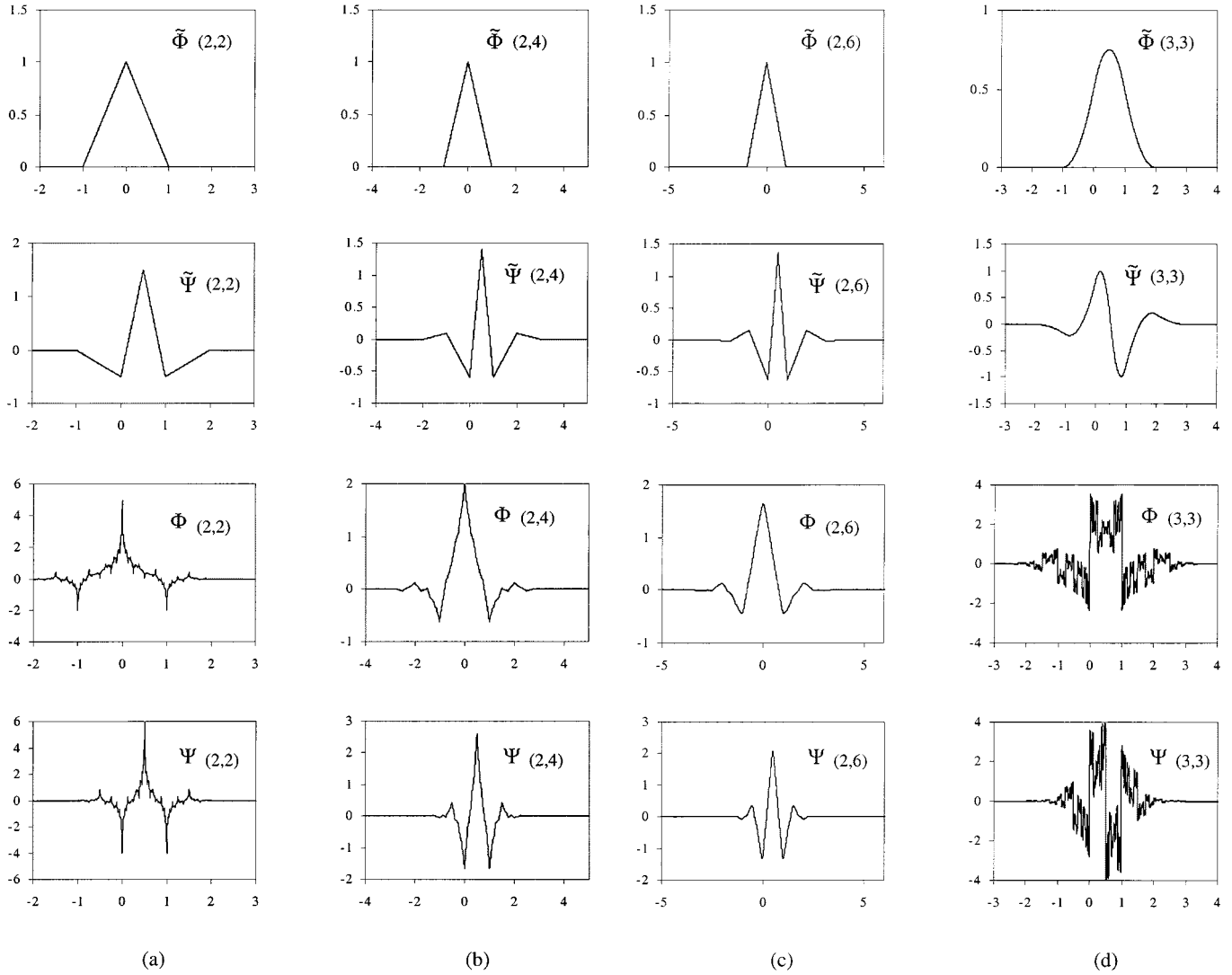
Fig. 1. *(Continued).* Scaling and wavelet functions and their duals for several families of CDF biorthogonal wavelet systems. In all cases, the graphs are approximations obtained by the cascade algorithm after eight iterations. (c) CDF $(2, 6)$. (d) CDF $(3, 3)$.

The method-of-moments procedure [16] is affected by testing Maxwell's equations with the scaling functions Φ_m. The resulting equations are

$$H_{k, m}^{\Phi} = H_{k-1, m}^{\Phi} + \frac{\Delta t}{\mu \Delta x} \sum_{i=1}^{n_a} a(i) \left(E_{k, m+i}^{\Phi} - E_{k, m-i+1}^{\Phi} \right)$$

(5a)

$$E_{k+1, m}^{\Phi} = E_{k, m}^{\Phi} + \frac{\Delta t}{\varepsilon \Delta x} \sum_{i=1}^{n_a} a(i) \left(H_{k, m+i-1}^{\Phi} - H_{k, m-i}^{\Phi} \right)$$

(5b)

where $a(i) = \int ((\partial \tilde{\Phi}_{m+i}(x))/(\partial x)) \Phi_{m+1/2}(x)\, dx$; Δx and Δt are the spatial and temporal steps, respectively. The number n_a, also called the "stencil size," equals half the number of the nonzero coefficients in the MRTD scheme. Note that we differentiate with respect to the dual function and, therefore, smoothness (differentiability) is imposed on such. The inner products are formed with the nondual functions, on which we, therefore, impose moment suppression.

The stability criterion for this algorithm was established in [3] and can be written as

$$\frac{c\Delta t}{\Delta x} \le \frac{1}{\displaystyle\sum_{i=1}^{n_a} |a(i)|}$$

(6)

where c is the phase velocity. The maximum values of $(c\Delta t)/(\Delta x)$ required by a stable algorithm (in one dimension) are given in Table I for different choices of the scaling functions. In two or three dimensions, these values must be adjusted by factors of $1/\sqrt{2}$ and $1/\sqrt{3}$, respectively [9].

B. Numerical Dispersion

In analyzing the numerical dispersion of the MRTD schemes, we consider a discretized monochromatic plane wave propagating in accord with the MRTD equations and study the phase

TABLE II
MRTD COEFFICIENTS FOR VARIOUS WAVELET BASES. (a) COEFFICIENTS $a(i)$. (b) COEFFICIENTS $b(i)$

i	CDF (2,2)	CDF (2,4)	CDF (2,6)	CDF (3,3)	Cubic spline Battle-Lemarie coefficients truncated at 10^{-3}
1	1.2291667	1.2918134	1.3110317	1.2918129	1.2918462
2	-0.0937500	-0.1371348	-0.1560124	-0.1371343	-0.1560761
3	0.0104167	0.0287617	0.0419962	0.0287618	0.0596391
4	0	-0.0034701	-0.0086543	-0.0034701	-0.0293099
5	0	0.0000080	0.0008308	0.0000080	0.0153716
6	0	0	0.0000109	0	-0.0081892
7	0	0	-0.0000000	0	0.0043788
8	0	0	0	0	-0.0023433
9	0	0	0	0	0.0012542

(a)

i	CDF (2,2)	CDF (2,4)	CDF (2,6)	CDF (3,3)	Cubic spline Battle-Lemarie coefficients truncated at 10^{-3}
1	1.4375000	1.6890090	1.8610039	1.6890090	2.4725388
2	0.0937500	0.1955818	0.2903309	0.1955818	0.9562282
3	-0.0104167	-0.0287622	-0.0426845	-0.0287618	0.1660587
4	0	0.0034701	0.0086545	0.0034701	0.0939244
5	0	-0.0000080	-0.0008308	-0.0000080	0.0031413
6	0	0	-0.0000109	0	0.0134936
7	0	0	0.0000000	0	-0.0028589
8	0	0	0	0	0.0027788
9	0	0	0	0	-0.0011295

(b)

error as compared with the continuous case. Following the procedure in [3], we obtain the following equation (for the 1-D case):

$$\frac{1}{q}\sin\frac{\pi q}{n_l} = \sum_{i=1}^{n_a} a(i)\sin\left[\frac{\pi u}{n_l}(2i-1)\right] \tag{7}$$

where $q = (c\Delta t)/(\Delta x)$ (the Courant number), $u = (\lambda_{\text{continuous}})/(\lambda_{\text{discrete}})$ (the ratio between the theoretical and numerical wavelength), and n_l are the number of sampling points per wavelength. Ideally, we should have $u = 1$. We measure the phase error (in degrees per wavelength) as $360(u - 1)$, where u represents the solution of the nonlinear equation (7) for a given discretization rate n_l.

TABLE II *(Continued)*.
MRTD COEFFICIENTS FOR VARIOUS WAVELET BASES (c) COEFFICIENTS $c(i)$. (d) COEFFICIENTS $d(i)$

i	CDF (2,2)	CDF (2,4)	CDF (2,6)	CDF (3,3)	Cubic spline Battle-Lemarie coefficients truncated at 10^{-3}
1	-0.1510417	-0.1569410	-0.1390804	0.2422510	-0.0465973
2	0.0833333	0.1363198	0.1482517	-0.3855128	0.0545394
3	-0.0052083	-0.0443966	-0.0742472	0.1597666	-0.0369996
4	0	0.0047841	0.0192157	-0.0178193	0.0205745
5	0	-0.0003301	-0.0026345	0.0013174	-0.0111530
6	0	0.0000008	0.0002887	-0.0000030	0.0059769
7	0	0	-0.0000146	0	-0.0032026
8	0	0	-0.0000002	0	0.0017141
9	0	0	0.0000000	0	-

(c)

i	CDF (2,2)	CDF (2,4)	CDF (2,6)	CDF (3,3)	Cubic spline Battle-Lemarie coefficients truncated at 10^{-3}
1	-0.0416667	-0.0726900	-0.0954514	-0.0181721	-0.0465973
2	0.0208333	0.0364721	0.0468862	0.0272902	0.0545394
3	0	-0.0000856	0.0005564	-0.0091396	-0.0369996
4	0	0	-0.0000002	0.0000214	0.0205745
5	0	0	0	0	-0.0111530
6	0	0	0	0	0.0059769
7	0	0	0	0	-0.0032026
8	0	0	0	0	0.0017141
9	0	0	0	0	-

(d)

In the following, we consider a few families of CDF biorthogonal wavelet functions and study the dispersion errors associated with their use in the MRTD algorithm. The results are also compared to those obtained with cubic-spline Battle–Lemarie wavelets and with the traditional Yee FDTD algorithm. For the CDF wavelet families, we use the notations CDF (α, β) [15], where the integers α and β are related to the lengths of the reconstruction and decomposition filters of the family [15], respectively (they are also related to the support extent of the scaling function Φ_m and the dual scaling function $\tilde{\Phi}_m$, respectively). Plots of the CDF families considered in this paper (including scaling and first-level wavelet functions) are given in Fig. 1. The scaling/wavelet functions in Fig. 1 were computed using the cascade algorithm [15]. The coefficients $a(i)$ were computed by
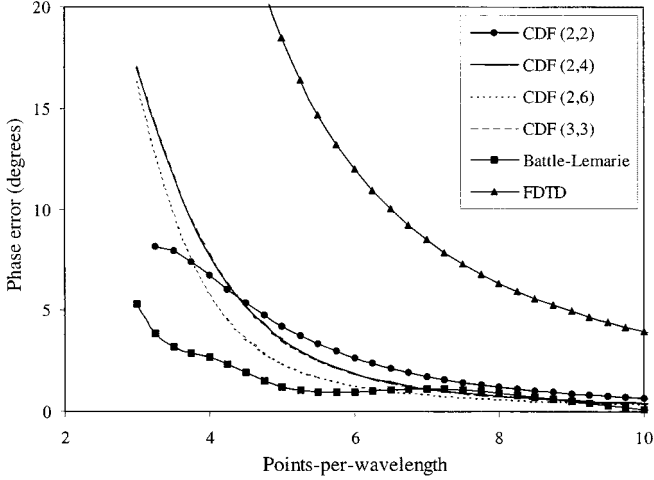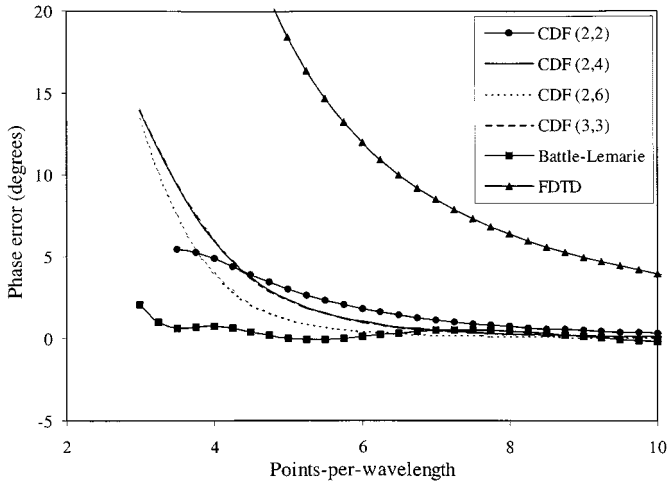
Fig. 2. Phase error (in degrees per wavelength) versus discretization rate for MRTD schemes using expansion of the fields in terms of scaling function only (at low resolution). For the MRTD schemes, the Courant number is $q = 0.25$, for FDTD, the Courant number is $q = 0.6$. 1-D propagation. The curves for CDF $(2, 4)$ and CDF $(3, 3)$ are on top of one another.

Fig. 4. Phase error (in degrees per wavelength) versus discretization rate for MRTD schemes using expansion of the fields in terms of scaling function only (at high resolution). For the MRTD schemes, the Courant number is $q = 0.25$, for FDTD, the Courant number is $q = 0.6$. 1-D propagation. The curves for CDF $(2, 4)$ and CDF $(3, 3)$ are on top of one another.

Fig. 3. Phase error (in degrees per wavelength) versus discretization rate for MRTD schemes using expansion of the fields in terms of scaling function only (at low resolution). For the MRTD schemes, the Courant number is $q = 0.1$, for FDTD, the Courant number is $q = 0.6$. 1-D propagation. The curves for CDF $(2, 4)$ and CDF $(3, 3)$ are on top of one another.
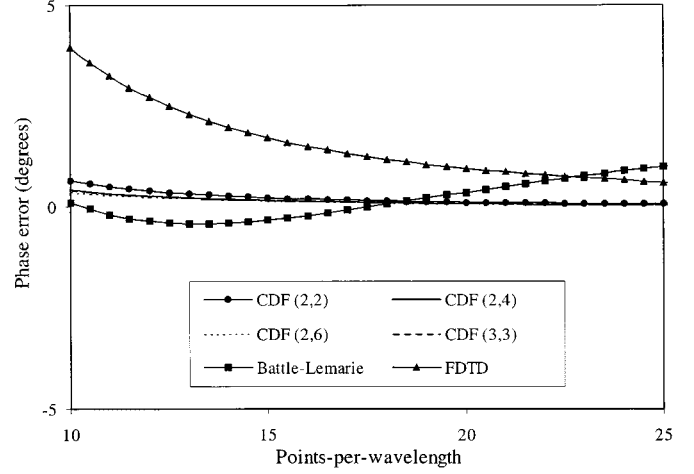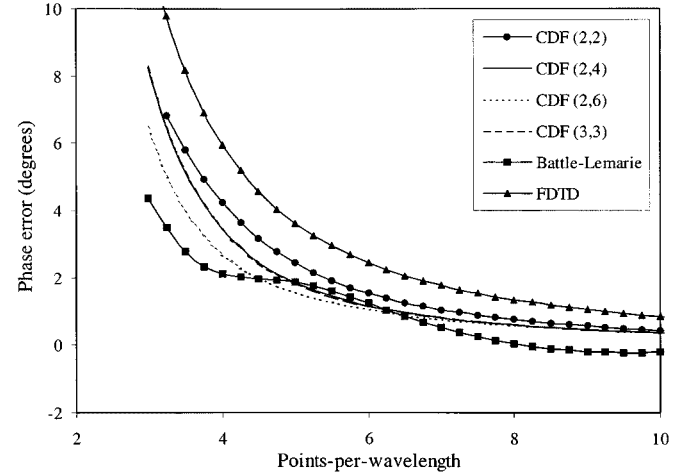

Fig. 5. Phase error (in degrees per wavelength) versus discretization rate for MRTD schemes using expansion of the fields in terms of scaling function only (at low resolution). For the MRTD schemes, the Courant number is $q = 0.25$, for FDTD, the Courant number is $q = 0.6$. 2-D propagation at $45°$. The curves for CDF $(2, 4)$ and CDF $(3, 3)$ are on top of one another.

numerical differentiation/integration and are given in Table II. Notice that, in some cases, the functions Φ_m can be very rough (we do not impose any smoothness condition on them, only moment suppression) and, therefore, they must be discretized very finely in order to obtain sufficient precision in the numerical integration (up to 20 levels of the cascade algorithm were used for six to seven decimal places). On the other hand, we notice that the dual scaling/wavelet functions are piecewise smooth and, therefore, the numerical differentiation is not a problem (actually it can be done in closed form for spline functions).

The dispersion curves for scaling-function field expansion are given in Figs. 2–5, in which the phase error is depicted as a function of the number of discretization points per wavelength. As a control, we plot the dispersion curves for the FDTD algorithm on the same graphs. It is important to mention that the errors are sensitive to the Courant number q. For all MRTD schemes

considered, we noticed that the phase error decreases when q is decreased (consistent with the results reported in [3]). However, for the FDTD algorithm, the opposite is true. In the following examples, we keep $q = 0.6$ for all the FDTD dispersion curves. More details on the influence of the Courant number on the FDTD dispersion curves can be found in [3]. In Fig. 2, we considered $q = 0.25$ for the MRTD schemes (since the stability limits are comparable for all MRTD schemes using scaling function expansions, we can directly compare them at the same Courant number). In Fig. 3, we lower the time step such that $q = 0.1$ for the same schemes, and in Fig. 4, we plot the same curves as in Fig. 2, but display curves for higher values of n_l (number of sample points per wavelength). The most striking aspect of the dispersion curves for the Battle–Lemarie system is that the error reaches a minimum and then increases as n_l is increased (we used a stencil size 9 for this MRTD scheme). This suggests that the error should increase at higher discretization

rates and that we would never reach the exact solution, no matter how finely we discretize the fields. However, we attribute this anomaly to the truncation of the MRTD coefficient sequence $a(i)$. Actually, it is easy to see that, in order to converge to the exact solution as $\Delta x \to 0$, we require

$$\sum_{i=1}^{n_a} a(i)(2i - 1) = 1. \tag{8}$$

The finite precision arithmetic used in computing the coefficients $a(i)$ leads to an error in satisfying this relationship, and it can be shown that this error is directly related to the phase error in the limit $\Delta x \to 0$. If we use a larger stencil size for the Battle–Lemarie MRTD scheme, this error can be reduced and the shape of the curves looks more similar to the ones obtained for the other MRTD schemes [3]. In fact, we noticed that the phase error in the case of the MRTD algorithms using biorthogonal wavelet expansion also does not converge exactly to zero in the limit $\Delta x \to 0$ (due to finite numerical precision), however, the errors are much smaller than in the Battle–Lemarie case. For comparison, the error associated with the coefficient computation is on the order of 10^{-6}, whereas the error associated with the coefficient sequence truncation (for the Battle–Lemarie scheme with stencil size 9) is on the order of 10^{-3}.

The behavior of the dispersion curves in the limit $\Delta x \to 0$ has theoretical value rather than a practical one since we are mainly interested in operating the MRTD algorithm at a discretization rate as low as possible. If we accept the phase error obtained for the FDTD scheme at ten points-per-wavelength, then we can use as few as three to five points-per-wavelength in the MRTD algorithm, depending on the choice of the basis and on the Courant number. The best performance appears to be provided by the cubic-spline Battle–Lemarie functions, at least at this level of discretization. However, these curves were obtained considering 1-D wave propagation. If we consider the two-dimensional (2-D) case, the dispersion error depends on the angle of propagation. In Fig. 5, we look at the phase errors for propagation at $45°$ for the same parameters as in Fig. 1. One can notice that now, at about five points per wavelength, the Battle–Lemarie scheme does not provide better accuracy than the biorthogonal MRTD schemes considered. Another interesting fact about these curves is the reduction of the error for the FDTD scheme at $45°$, when a Courant number of $q = 0.6$ is employed. In fact, it is well known that, for a Courant number close to the stability limit ($q = 1/\sqrt{2}$ in two dimensions), the dispersion error of the Yee algorithm vanishes for propagation at $45°$ [9]. This discussion suggests that one set of curves at one angle and one Courant number do not completely characterize the error obtained in a complex scattering configuration. In the case of the Battle–Lemarie MRTD scheme, we expect spurious errors caused by the truncation of the coefficient sequence. On the other hand, the performance of the biorthogonal MRTD schemes should be more predictable since the precision errors involved in arithmetic computations are much smaller. Finally, we note that all the above dispersion analyses were performed at Courant numbers that guarantee stability in 2-D configurations for all MRTD and FDTD schemes (in fact, the 1-D cases correspond to 2-D propagation along one of the Cartesian axes).

C. Computational Complexity

Another issue to be addressed is the number of floating-point calculations involved in each update equation. If the stencil size of the MRTD algorithm is n_a, using only scaling functions, then in order to achieve a similar number of computations with the Yee FDTD scheme for the same problem, we must reduce the number of cells in one direction by a factor of n_a in one dimension, $\sqrt{n_a}$ in two dimensions, and $\sqrt[3]{n_a}$ in three dimensions. It is easy to see that the savings of the MRTD scheme become more important as the number of spatial dimensions is increased. In the following, we make the comparisons with the Yee scheme employing ten points per wavelength. Since the Battle–Lemarie scheme needs at least $n_a = 9$, for this wavelet choice, the MRTD algorithm becomes more efficient than FDTD (in terms of computational time) only in a three-dimensional (3-D) configuration. Increasing the stencil size for the Battle–Lemarie scheme does not reduce the dispersion error significantly at low discretization rates [3], but it does increase the computation time. We also tried to decrease the stencil size of the Battle–Lemarie scheme to four, but the results in terms of numerical dispersion were very poor. The most economical MRTD scheme from this point-of-view appears to be the CDF $(2, 2)$ basis, which has a stencil size of $n_a = 3$ and offers phase accuracy comparable with the other MRTD schemes. It can also be noticed that increasing the support of the scaling and wavelet functions in the CDF families does not lead to significant improvements in terms of phase error, but could increase the computation time significantly. The size of the time step is also important in evaluating the total CPU time. For all MRTD schemes, the accuracy is better as the time step is decreased. However, this increases the computational time necessary to obtain the numerical solution. Therefore, a tradeoff must be achieved between the accuracy of the scheme and total number of time steps (notice that, in the FDTD case, this tradeoff is not necessary because choosing the Courant number close to the stability limit is nearly optimal).

IV. BIORTHOGONAL MRTD USING THE FIRST LEVEL OF WAVELET FUNCTIONS

In this section, we perform a similar error analysis of the MRTD algorithm, considering an expansion of the fields in terms of scaling functions and a single level of wavelet functions. The formulation depends on whether the wavelet functions (and their duals) are symmetric or antisymmetric about one-half (see Fig. 1). If the wavelets are symmetric (e.g., CDF $(2, 2)$, $(2, 4)$, $(2, 6)$, and cubic-spline Battle–Lemarie), then, at cell m (in one dimension), the component H^Ψ occupies the same position as the component E^Φ, whereas E^Ψ occupies the same position as H^Φ (we call the "position" of a field component, the coordinate where the scaling or wavelet function associated with it peaks out). If the wavelets are antisymmetric [e.g., CDF $(3, 3)$], then, at cell m, the component E^Ψ aligns with the component E^Φ, whereas H^Ψ aligns with H^Φ. The

MRTD update equations in the symmetric case are (for 1-D propagation)

$$H^{\Phi}_{k,m} = H^{\Phi}_{k-1,m} + \frac{\Delta t}{\mu \Delta x}$$
$$\cdot \left(\sum_{i=1}^{n_a} a(i) \left(E^{\Phi}_{k,m+i} - E^{\Phi}_{k,m-i+1} \right) \right.$$
$$\left. + \sum_{i=1}^{n_c} c(i) \left(E^{\Psi}_{k,m+i} - E^{\Psi}_{k,m-i} \right) \right) \qquad (9a)$$

$$H^{\Psi}_{k,m} = H^{\Psi}_{k-1,m} + \frac{\Delta t}{\mu \Delta x}$$
$$\cdot \left(\sum_{i=1}^{n_d} d(i) \left(E^{\Phi}_{k,m+i} - E^{\Phi}_{k,m-i} \right) \right.$$
$$\left. + \sum_{i=1}^{n_b} b(i) \left(E^{\Psi}_{k,m+i-1} - E^{\Psi}_{k,m-i} \right) \right) \qquad (9b)$$

$$E^{\Phi}_{k+1,m} = E^{\Phi}_{k,m} + \frac{\Delta t}{\varepsilon \Delta x}$$
$$\cdot \left(\sum_{i=1}^{n_a} a(i) \left(H^{\Phi}_{k,m+i-1} - H^{\Phi}_{k,m-i} \right) \right.$$
$$\left. + \sum_{i=1}^{n_c} c(i) \left(H^{\Psi}_{k,m+i} - H^{\Psi}_{k,m-i} \right) \right) \qquad (9c)$$

$$E^{\Psi}_{k+1,m} = E^{\Psi}_{k,m} + \frac{\Delta t}{\varepsilon \Delta x}$$
$$\cdot \left(\sum_{i=1}^{n_d} d(i) \left(H^{\Phi}_{k,m+i} - H^{\Phi}_{k,m-i} \right) \right.$$
$$\left. + \sum_{i=1}^{n_b} b(i) \left(H^{\Psi}_{k,m+i} - H^{\Psi}_{k,m-i+1} \right) \right) \qquad (9d)$$

where $b(i) = \int ((\partial \tilde{\Psi}_{m+i}(x))/(\partial x)) \Psi_{m+1/2}(x)\, dx$, $c(i) = \int ((\partial \tilde{\Psi}_{m+i}(x))/(\partial x)) \Phi_{m+1/2}(x)\, dx$ (we have $c(0) = 0$) and $d(i) = \int ((\partial \tilde{\Phi}_{m+i}(x))/(\partial x)) \Psi_{m-1/2}(x)\, dx$ (we have $d(0) = 0$). Notice that we have dropped the index zero indicating the wavelet level. For the biorthogonal MRTD schemes, the $c(i)$ and $d(i)$ coefficient have different values, unlike the Battle-Lemarie

scheme [1], which uses orthonormal basis functions. For the antisymmetric case, the corresponding equations are

$$H^{\Phi}_{k,m} = H^{\Phi}_{k-1,m} + \frac{\Delta t}{\mu \Delta x}$$
$$\cdot \left(\sum_{i=1}^{n_a} a(i) \left(E^{\Phi}_{k,m+i} - E^{\Phi}_{k,m-i+1} \right) \right.$$
$$\left. + \sum_{i=1}^{n_c} c(i) \left(E^{\Psi}_{k,m+i} + E^{\Psi}_{k,m-i+1} \right) \right) \qquad (10a)$$

$$H^{\Psi}_{k,m} = H^{\Psi}_{k-1,m} + \frac{\Delta t}{\mu \Delta x}$$
$$\cdot \left(\sum_{i=1}^{n_d} d(i) \left(E^{\Phi}_{k,m+i} + E^{\Phi}_{k,m-i+1} \right) \right.$$
$$\left. + \sum_{i=1}^{n_b} b(i) \left(E^{\Psi}_{k,m+i} - E^{\Psi}_{k,m-i+1} \right) \right) \qquad (10b)$$

$$E^{\Phi}_{k+1,m} = E^{\Phi}_{k,m} + \frac{\Delta t}{\varepsilon \Delta x}$$
$$\cdot \left(\sum_{i=1}^{n_a} a(i) \left(H^{\Phi}_{k,m+i-1} - H^{\Phi}_{k,m-i} \right) \right.$$
$$\left. + \sum_{i=1}^{n_c} c(i) \left(H^{\Psi}_{k,m+i-1} + H^{\Psi}_{k,m-i} \right) \right) \qquad (10c)$$

$$E^{\Psi}_{k+1,m} = E^{\Psi}_{k,m} + \frac{\Delta t}{\varepsilon \Delta x}$$
$$\cdot \left(\sum_{i=1}^{n_d} d(i) \left(H^{\Phi}_{k,m+i-1} + H^{\Phi}_{k,m-i} \right) \right.$$
$$\left. + \sum_{i=1}^{n_b} b(i) \left(H^{\Psi}_{k,m+i-1} - H^{\Psi}_{k,m-i} \right) \right) \qquad (10d)$$

where the coefficients $b(i)$, $c(i)$, and $d(i)$ have the same expressions as above. Their values are listed in Table II for all the wavelet families considered above.

The stability criterion can be written as (11), shown at the bottom of this page [3], in which $n = \max(n_a, n_b)$. The maximum values of $(c\Delta t)/(\Delta x)$ required by a stable algorithm (in one dimension) are given in Table I.

To analyze the dispersion properties of the MRTD scheme using one level of wavelets, we plot similar phase error graphs

$$\frac{c\Delta t}{\Delta x} \leq \frac{\sqrt{2}}{\sqrt{\left(\sum_{i=1}^{n_a} |a(i)| \right)^2 + \left(\sum_{i=1}^{n_b} |b(i)| \right)^2 + 2 \sum_{i=1}^{n_c} |c(i)| \sum_{i=1}^{n_d} |d(i)|} + \left(\sum_{i=1}^{n} |a(i) + b(i)| \right) \sqrt{\left(\sum_{i=1}^{n} |a(i) - b(i)| \right)^2 + 4 \sum_{i=1}^{n_c} |c(i)| \sum_{i=1}^{n_d} |d(i)|}} \qquad (11)$$

versus the discretization rate, as discussed in the previous section. The dispersion relationship for the numerical MRTD solution of Maxwell's equations can be written as

$$1 - \left(s_a^2 + s_b^2 + s_c s_d\right) + \left(s_a s_b - s_c s_d\right)^2 = 0 \qquad (12)$$

where

$$s_a = q \frac{\sum_{i=1}^{n_a} a(i) \sin\left[\frac{\pi u}{n_l}(2i-1)\right]}{\sin \frac{\pi q}{n_l}} \qquad (13a)$$

$$s_b = q \frac{\sum_{i=1}^{n_b} b(i) \sin\left[\frac{\pi u}{n_l}(2i-1)\right]}{\sin \frac{\pi q}{n_l}} \qquad (13b)$$

$$s_c = q \frac{\sum_{i=1}^{n_c} c(i) \frac{\sin}{\cos}\left(\frac{\pi u}{n_l}2i\right)}{\sin \frac{\pi q}{n_l}} \qquad (13c)$$

$$s_d = q \frac{\sum_{i=1}^{n_d} d(i) \frac{\sin}{\cos}\left(\frac{\pi u}{n_l}2i\right)}{\sin \frac{\pi q}{n_l}}. \qquad (13d)$$

In the numerators of s_c and s_d, we take sine for symmetric wavelet systems and cosine for antisymmetric wavelet systems. The graphs in Fig. 6 were obtained for $q = 0.25$ (which insures that all schemes are stable) and the same families of wavelets as in the previous sections. In theory, by introducing a level of wavelets, the resolution of the MRTD schemes should double. However, the curves in Fig. 6 show a modest reduction in the phase error for the Battle-Lemarie MRTD scheme (stencil size 9) when wavelets are considered, as compared to the case where the expansion was provided by scaling functions only. One explanation for this result can be again provided by the truncation of the MRTD coefficient sequence. However, we conjecture that the principal reason for the small difference between the two Battle–Lemarie MRTD schemes (one using scaling functions only and the other using scaling plus first-level wavelet functions), when they both use the same Courant number, is the fact that, in the second case, we operate much closer to the stability limit (see Table I). The curves in Fig. 6 indicate, against expectations, that the performance decreases as the order of the wavelet system increases. However, we can explain this by taking into account that the numerical dispersion error is also a function of the Courant number. One can notice that, e.g., in the Battle–Lemarie scheme, $q = 0.25$ is very close to the stability limit, whereas for CDF $(2, 2)$, this value is well below the stability limit of the scheme. As mentioned in Section III, the errors decrease with q. In Fig. 7, we consider the same dispersion curves, but operate all MRTD schemes at Courant numbers equal to 95% of their stability limits. Now the dispersion performances of the schemes are as expected (i.e., the higher order schemes offer better performance). However, the comparison we make in Fig. 6 is meaningful because, in
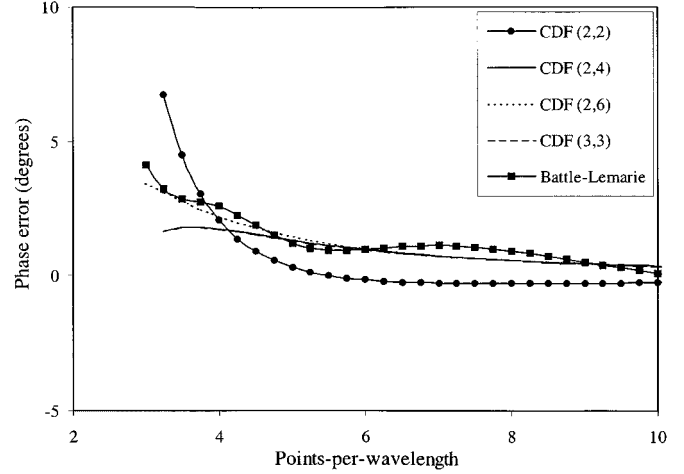

Fig. 6. Phase error (in degrees per wavelength) versus discretization rate for MRTD schemes using expansion of the fields in terms of scaling and one level wavelet functions. For all schemes, the Courant number is $q = 0.25$. 1-D propagation. The curves for CDF $(2, 4)$ and CDF $(3, 3)$ are on top of one another.
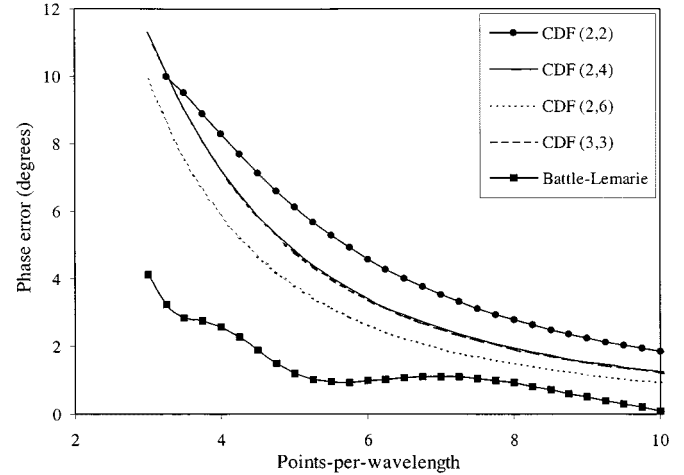

Fig. 7. Phase error (in degrees per wavelength) versus discretization rate for MRTD schemes using expansion of the fields in terms of scaling and one level wavelet functions. For all schemes, the Courant number is 95% of the stability limit. 1-D propagation. The curves for CDF $(2, 4)$ and CDF $(3, 3)$ are on top of one another.

this case, all MRTD schemes have the same time step. The graphs in this figure clearly show that, for the same time step, the biorthogonal schemes have lower numerical dispersion than the Battle–Lemarie scheme.

The stencil sizes for the coefficient sequences $a(i), b(i), c(i)$, and $d(i)$ are given in Table III. Once again, the biorthogonal MRTD schemes with low-order support, e.g., CDF $(2, 2)$ and CDF $(2, 4)$, are the most efficient in terms of the number of computations (while providing better dispersion performance than the Battle–Lemarie basis for a similar Courant number). In this case, where one scaling and one level wavelet functions are employed, the number of calculations in the update equation for one field component is about $n_a + n_b + n_c + n_d$ times larger than the ones required by FDTD. Again, the savings of the MRTD algorithm increase with the number of spatial dimensions. We should also mention that the differences in the Courant number for the schemes using scaling plus one level wavelet functions

TABLE III
STENCIL SIZES FOR DIFFERENT MRTD SCHEMES

	CDF (2,2)	CDF (2,4)	CDF (2,6)	CDF (3,3)	Cubic spline Battle-Lemarie coefficients truncated at 10^{-3}
n_a	3	5	7	5	9
n_b	3	5	7	5	9
n_c	3	6	9	6	8
n_d	2	3	4	4	8

TABLE IV
RESONANT FREQUENCIES FOR AN AIR-FILLED METALLIC CAVITY (ALL FREQUENCIES IN MEGAHERTZ)

Analytic	S-MRTD				W-MRTD				FDTD
	CDF (2,2)	CDF (2,4)	CDF (2,6)	Battle-Lemarie	CDF (2,2)	CDF (2,4)	CDF (2,6)	Battle-Lemarie	
150.00	150.11	150.10	150.11	150.22	150.01	150.01	150.01	150.14	149.60
167.71	167.87	167.85	167.86	168.14	167.72	167.71	167.73	168.01	167.43
270.42	271.11	271.05	271.03	270.79	270.50	270.51	270.51	270.25	269.63
300.00	301.12	300.92	300.88	300.66	300.05	300.15	300.15	299.92	296.81

are significant, as one compares, e.g., the CDF $(2, 2)$ scheme with the Battle–Lemarie scheme (see Table I). This means that, in the former algorithm, we can choose a time step that is more than double the one used by the latter scheme, and still maintain stability. However, increasing the time step adversely affects the accuracy of the algorithm (compare Figs. 6 and 7). Finally, we note that, when using scaling functions and wavelets (here, a single wavelet level), the MRTD also has the added benefit of multiresolution. In this context, scaling functions alone can be used in regions in which the fields vary relatively slowly, with wavelets added locally in regions of fast field variation.

V. NUMERICAL EXAMPLE

To address implementation of the MRTD with CDF biorthogonal wavelets, we consider a simple electromagnetic problem, i.e., studying the resonant frequencies of an air-filled metallic cavity, in a manner similar to the example in [1]. We considered a 2-D cavity of 1 m × 2 m (with perfectly conducting walls) discretized with a grid step of $\Delta x = 0.1$ m for all versions of FDTD/MRTD models. We performed simulations using the MRTD algorithm based on scaling functions alone (S-MRTD with the notations in [1]) and the same algorithm based on scaling and first level wavelet functions (W-MRTD). In the latter case, we employed the full expansion in both directions,

uniformly throughout the whole computational domain. The Battle–Lemarie MRTD scheme uses a stencil size 9 (as given in Table III). We also implemented the same problem with the Yee FDTD algorithm. The Courant numbers were $q = 0.42$ for S-MRTD, $q = 0.17$ for W-MRTD (same for all wavelet bases), and $q = 0.6$ for FDTD. We considered four resonant frequencies, which were obtained either in TE or TM polarizations. We chose a relatively high discretization rate in order to have a number of cells larger than the stencil size of any scheme in each direction. In this manner, only one image of the cavity is required at each metallic wall in order to enforce the boundary conditions. The numerical results are given in Table IV.

Based on these results, we can conclude that all MRTD schemes provide good accuracy in measuring the resonant frequencies of the cavity, and they all perform better than FDTD. The differences between the various schemes are small—some model the higher frequencies more accurately, whereas others do better on the lower frequencies. As expected, adding one level of wavelets resulted in improved precision. However, one should be aware that the Courant number for W-MRTD is different from that used by the S-MRTD (the time steps are different). Also, based on the discussion in the previous section, the numerical results confirm that, for the same Courant number, the CDF $(2, 2)$ W-MRTD scheme provides the most accurate results. We emphasize that the point of this

numerical experiment is simply to underscore that the MRTD is implemented easily, using either CDF biorthogonal wavelets or the orthogonal Battle-Lemarie wavelets. In particular, in these computations, we have not focused on the reduced spatial discretization afforded by the various MRTD schemes, this issue having been addressed in the dispersion studies.

VI. CONCLUSIONS

In this paper, we have formulated the MRTD algorithm using biorthogonal wavelet families. We chose the CDF biorthogonal systems because they fit well with the requirements for an efficient MRTD scheme: maximum number of vanishing moments for the wavelet function (for a given support), good regularity for the dual-wavelet function, and compact support. We analyzed the dispersion properties of the MRTD scheme for a few families of CDF biorthogonal wavelets and compared them with the cubic-spline Battle–Lemarie scheme. Although, in theory, the latter should perform better in terms of numerical dispersion, the error associated with truncating the MRTD coefficient sequence vitiates the accuracy of the scheme, when finite arithmetic precision is considered. The effect is more evident when we consider field expansion in terms of scaling and first-level wavelet functions. The biorthogonal wavelet systems do not present this problem, due to their compact support, although high precision is required in the MRTD coefficient calculation in order to minimize arithmetic inaccuracies. Also, the compact support of the biorthogonal wavelets reduces the total CPU time relative to the Battle-Lemarie wavelets for similar levels of phase error.

REFERENCES

[1] M. Krumpholz and L. Katehi, "MRTD: New time-domain schemes based on multiresolution analysis," *IEEE Trans. Microwave Theory Tech.*, vol. 44, pp. 555–571, Apr. 1996.

[2] E. M. Tentzeris, R. L. Robertson, and L. Katehi, "PML absorbing boundary conditions for the characterization of open microwave circuit components using multiresolution time domain techniques (MRTD)," *IEEE Trans. Antennas Propagat.*, vol. 47, pp. 1709–1716, Nov. 1999.

[3] E. M. Tentzeris, R. L. Robertson, J. Harvey, and L. Katehi, "Stability and dispersion analysis of Battle–Lemarie based MRTD schemes," *IEEE Trans. Microwave Theory Tech.*, vol. 47, pp. 1004–1013, July 1999.

[4] T. Dogaru and L. Carin, "Application of multiresolution time-domain schemes to two-dimensional electromagnetic scattering problems," *IEEE Trans. Antennas Propagat.*, submitted for publication.

[5] ——, "Multiresolution time-domain analysis of scattering from a rough dielectric surface," *Radio Sci.*, vol. 35, pp. 1279–1292, Nov.–Dec. 2000.

[6] T. Dogaru, "Modeling and signal processing for electromagnetic subsurface sensing," Ph.D. dissertation, Dept. Elect. Comput. Eng., Duke Univ., Durham, NC, 1999.

[7] K. S. Yee, "Numerical solution of initial boundary value problems involving Maxwell's equations in isotropic media," *IEEE Trans. Antennas Propagat.*, vol. AP-14, pp. 302–307, May 1966.

[8] K. S. Kunz and R. J. Luebbers, *The Finite Difference Time Domain Method for Electromagnetics*. Boca Raton, FL: CRC Press, 1993.

[9] A. Taflove, *Computational Electrodynamics: The Finite-Difference Time-Domain Method*. Norwood, MA: Artech House, 1995.

[10] P. G. Petropoulos, "Phase error control for FDTD methods of second and fourth order accuracy," *IEEE Trans. Antennas Propagat.*, vol. 42, pp. 859–862, June 1994.

[11] M. F. Hadi and M. Piket-May, "A modified FDTD (2,4) scheme for modeling electrically large structures with high-phase accuracy," *IEEE Trans. Antenna Propagat.*, vol. 45, pp. 254–264, Feb. 1997.

[12] M. W. Chevalier, R. J. Luebbers, and V. P. Cable, "FDTD local grid with material traverse," *IEEE Trans. Antennas Propagat.*, vol. 45, pp. 411–421, Mar. 1997.

[13] M. Okoniewski, E. Okoniewska, and M. A. Stuchly, "Three-dimensional subgridding algorithm for FDTD," *IEEE Trans. Antennas Propagat.*, vol. 45, pp. 422–429, Mar. 1997.

[14] M. J. White, M. F. Iskander, and Z. Huang, "Development of a multigrid FDTD Code for three-dimensional applications," *IEEE Trans. Antennas Propagat.*, vol. 45, pp. 1512–1517, Oct. 1997.

[15] I. Daubechies, *Ten Lectures on Wavelets*. Philadelphia, PA: SIAM, 1992.

[16] R. F. Harrington, *Field Computation by Moment Methods*. Melbourne, FL: Krieger, 1968.

[17] Y. W. Cheong, Y. M. Lee, K. H. Ra, J. G. Kang, and C. C. Shin, "Wavelet–Galerkin scheme of time-dependent inhomogeneous electromagnetic problems," *IEEE Microwave Guided Wave Lett.*, vol. 9, pp. 297–299, Aug. 1999.

[18] M. Fujii and W. J. R. Hoefer, "Dispersion of time domain wavelet Galerkin method based on Daubechies' compactly supported scaling functions with three and four vanishing moments," *IEEE Microwave Guided Wave Lett.*, vol. 10, pp. 125–127, Apr. 2000.

[19] J. Gotze, J. E. Odegard, P. Rieder, and C. S. Burrus, "Approximate moments and regularity of efficiently implemented orthogonal wavelet transforms," in *Proc. IEEE Int. Circuits Syst. Symp. Dig.*, May 1996, pp. 405–408.

Traian Dogaru (S'96–M'99) was born in Bucharest, Romania, in 1966. He received the Engineering degree from the Polytechnic University of Bucharest, Bucharest, Romania, in 1990, the M.S. degree in electrical engineering and the Ph.D. degree from Duke University, Durham, NC, in 1997 and 1999, respectively.

From 1992 to 1995, he has held different engineering positions in the magnetic recording industry. He is currently a Research Associate at Duke University, where his main research interests are in electromagnetic wave theory, computational electromagnetics, rough surface scattering and radar-related signal processing.

Lawrence Carin (S'85–M'85–SM'96–F'01) was born March 25, 1963, in Washington, DC. He received the B.S., M.S., and Ph.D. degrees in electrical engineering from the University of Maryland at College Park, in 1985, 1986, and 1989, respectively.

In 1989, he joined the Electrical Engineering Department, Polytechnic University, Brooklyn, NY, as an Assistant Professor and, in 1994, became an Associate Professor. In September 1995, he joined the Electrical Engineering Department, Duke University, Durham, NC, where he is currently a Professor. His current research interests include short-pulse scattering, subsurface sensing, and wave-based signal processing.

Dr. Carin is a member of Tau Beta Pi and Eta Kappa Nu. He is the principal investigator of a Multidisciplinary University Research Initiative (MURI) on demining. He is currently an associate editor for the IEEE TRANSACTIONS ON ANTENNAS AND PROPAGATION.